Brain Tumor Segmentation in MRI Scans Using Convolutional Neural Networks

Maja Pantić

***Abstract*—In this paper an algorithm for segmentation of brain tumor lesions in magnetic resonance images (MRI) using convolutional neural networks (CNN) is proposed. Precise determination of brain tumor regions is important for diagnosis, treatment choice and patient follow-up. The realized CNN model has the U-Net architecture, which is able to simultaneously extract structure characteristics and their precise locations in the input image. The U-Net is applied on the scans of high-grade glioma patients. The resulting segmentation is evaluated using Dice coefficient and the median Dice values achieved on the test images are 0.83, 0.58 and 0.74 on the whole tumor, active tumor and core tumor region respectively.**

***Index Terms*—brain tumor segmentation; biomedical image processing; convolutional neural networks; U-Net architecture.**

I. Introduction

BRAIN tumor represents the uncontrolled growth of abnormal cells within the brain tissues [1]. Brain tumors can be malignant, when they are referred to as cancer, or benign. Both types of tumor can harm the proper functioning of the affected brain region and need adequate treatment [1].

There are more than 130 types of brain tumors [2]. Based on the organ in which they first appear, brain tumors are classified either as primary or secondary (metastatic) tumors. Primary brain tumors appear in the brain and can spread to other regions in the brain or spinal cord, while metastatic tumors first appear in other body organs and spread to the brain tissues. The most common primary brain tumor type in adults is astrocytoma or glioblastoma multiforme (GBM). GBM is a type of glioma brain tumor which is formed of glial cells, supporting cells of the central nervous system [3].

According to the World Health Organization, the classification of the brain and spinal cord tumors is done on the molecular and histological level [4]. Brain tumors are categorized in four different grades based on the abnormality of tumor cells observed under a microscope and the pace of their growth and spreading. Grade I tumors, also referred to as low-grade tumors, grow and spread slower than higher grade tumors, rarely affect the surrounding tissues and can be cured if completely removed by surgery. Tumors classified as grade IV, also referred to as high-grade tumors, are the most aggressive brain tumor types, as they grow and spread at a very rapid pace and usually cannot be cured [1, 4].

Medical imaging modalities used in medical practice for brain tumor diagnosis are: computerized tomography (CT), magnetic resonance imaging (MRI), single photon emission computed tomography (SPECT) and positron emission tomography (PET). Identifying the exact position, shape and size of tumor lesions in the obtained images or 3D volumes is crucial for correct diagnosis and choice of adequate treatment methods [1]. Therefore, development of image processing techniques which automatically analyze tumor scans with the aim to segment the tumor regions and identify tumor substructures are of great importance, as they could improve and accelerate the process of diagnosis, treatment choice and patients' follow-up care [5]. Automatic segmentation of brain tumor lesions is a challenging task, as the tumor lesions can be of different shape and size and can appear in any region of the brain, as well as vary in pixel intensities in the scanned images, due to the usage of different modalities and scanning devices. Thus, automatic brain tumor segmentation techniques cannot assume any information about the position, size and pixel intensity of tumor lesions in scanned images [5].

Based on the type of information used for the segmentation of tumor regions, segmentation methods can be categorized as either generative probabilistic or discriminative [5]. Generative probabilistic methods combine knowledge of anatomical brain models with the spatial distribution of different tissue types in the brain and can usually generalize well on the previously unseen scans. Discriminative methods do not require information related to the brain structure and they segment the tumor lesions by learning the characteristics from the images and their relations to the segmentation labels manually annotated by the experts. Such methods require large datasets for the training purposes. Segmentation techniques which combine the characteristics of both generative probabilistic and discriminative methods are called generative-discriminative methods [5].

Starting from 2012, the Brain Tumor Image Segmentation Challenge (BRATS) is organized annually with the conjunction of the international Medical Image Computing and Computer Assisted Interventions (MICCAI) conference [6], with the aim of proposing different brain tumor segmentation methods and comparing the results on the commonly used publicly available dataset and using the common protocol for the results evaluation [5, 7]. Since 2014, discriminative methods based on convolutional neural networks (CNNs) have become the most commonly proposed segmentation methods in the BRATS challenges, with a number of novel network architectures as well as their variations suggested every year. CNN models trained on extracted 2 dimensional (2D) or 3 dimensional (3D) image

Maja Pantić is a student of the Master's study program at School of Electrical Engineering, University of Belgrade, 73 Bulevar kralja Aleksandra, 11020 Belgrade, Serbia (e-mail: pm193067m@student.etf.bg.ac.rs).

patches aim to predict the class of the central pixel in the patch while learning local relations between the pixels inside the extracted patch regions [8-12]. In [13] a cascaded two-pathway CNN architecture was proposed, where each path extracts features respectively from the larger-size and the smaller-size 2D patches extracted around the central pixel, so that the network can make predictions based both on the local and more global features. Fully convolutional neural networks (FCNN) do not contain dense neural layers and can produce dense segmentation of the whole images or image patches given at the network input. Number of methods proposed variations of different FCNN architectures, such as DeepMedic [14-16], VGG [15], SegNet [17, 18], U-Net [19-23] and V-Net [24, 25]. DeepMedic is a FCNN architecture with 2 parallel paths which process the input 3D patches extracted from the image at different pixel resolutions, while SegNet, VGG, U-Net and V-Net can be modified to process either whole image slices or 3D patches. Several methods propose cascaded network architectures, where the output of one network architecture is used as the input into the next network, thus achieving segmentation results through several phases [25-28]. In [29] several network architectures were trained independently and then used to form the network ensemble for final segmentation results by averaging the outputs of individual models.

In this paper the automatic discriminative method for glioma brain tumor segmentation in multimodal MR images based on the U-Net architecture of CNN is described. In Section II, the proposed CNN architecture, dataset used and the details on the algorithm implementation are described. Section III represents the segmentation results. Finally, Section IV gives brief conclusion of the proposed method, as well as possible ways of future improvements of the results.

II. The Method

A. The Database

Database used for the training and testing of the proposed segmentation algorithm is the publicly available database of MRI scans of glioma patients [30] used in the BRATS challenges 2015 and 2016 [5, 31]. The training and validation dataset contains 220 scans of high-grade glioma patients and 54 scans of low-grade glioma patients, while the testing dataset consists of 110 mixed scans of both high-grade and low-grade glioma patients. For each patient, there are 155 2D images in axial plane available, acquired with each of following MRI contrasts: T1-weighted, T1-weighted contrast-enhanced (T1c), T2-weighted and T2-weighted FLAIR. The training and validation dataset also contains masks with annotated labels of the tumor structures for all patients. All scans in the database were anonymized, scull stripped, co-registered to corresponding T1c scans and were set to the 1 mm^3 spatial resolution using linear interpolation.

The scans were manually annotated by the expert radiologists, based on the radiological criteria, so that the annotated structures belong to visually separable structures and do not strictly represent different biological structures within the brain. The tumor structures in the images are divided into four categories: edema, non-enhancing core, enhancing core and necrotic core. The annotation masks are the same size as the MRI scans and contain the following pixel-wise labels: 0 – background, 1 – necrotic core, 2 – edema, 3 – non-enhancing core, 4 – enhancing core. The enhancing core can be extracted on the high-grade glioma scans solely. The extracted tumor structures are further grouped into the following tumor regions:

- whole tumor region, which contains all four tumor structures;
- tumor core, which contains necrotic core, non-enhancing core and enhancing core;
- active tumor region, which contains enhancing core.

B. U-Net architecture

The U-Net architecture is the CNN architecture which, for the image given at its input, returns as the output the map of probabilities for each image pixel to be belonging to each of the considered segmentation classes. It was first proposed in [32], where it was used for the segmentation of the biomedical images: scans of neural structures obtained with an electron microscope and cell images obtained with a light microscope. Originally proposed U-Net architecture, as well as its modifications, found application in many other problems of biomedical image segmentation [19-23, 27, 28, 33-35]. Compared to many other CNN architectures used for segmentation purposes, the main advantage of the U-Net architecture is that it can take the whole image as its input, instead of taking various patches from the image. Thus, the network training process becomes faster and the problem of simultaneous feature extraction and their precise localization is avoided [32].

U-Net is a fully convolutional neural network. It consists of the two symmetric paths of convolutional layers, the contracting path and the expansive path, which can together be schematically represented to form the shape of the letter "U". The aim of the contracting path is to capture context in the image and it has the typical form of the CNN. Its main block consists of two convolutional layers, with activation function applied to the output of each of them and max pooling operation applied after the 2^{nd} convolutional layer. Every succeeding layer in the contracting path uses the doubled number of convolutional filters compared to the preceding layer. The aim of the expansive path is to precisely locate the captured details in the image. Each layer of the expansive path has the input formed by the concatenation of the output of the symmetric layer from the contracting path and the up-sampled output from the previous layer of the expansive path. On such formed input tensor, similarly as in the contracting path, two convolutional layers, each followed by activation functions, are applied and the result represents one of the inputs to the next layer of the expansive path. In the last layer of the expansive path an additional convolution operation is applied after the double convolutional layers and its output represents the map consisting of the probabilities for

each pixel in the input image to be belonging to different segmentation classes. The number of convolutional filters applied in the last convolution operation equals the number of different segmentation classes in the input image [32].

The U-Net architecture implemented in this paper, schematically represented in Fig. 1, resembles the original U-Net architecture, with several changes in the network architecture. It contains four symmetric layers in both the contracting and the expansive path, while the output of the 5th layer in the contracting path is up-sampled and concatenated to the output of the 4th layer in contracting path to form the input to the deepest layer of the expansive path. Different from the original U-Net architecture, the convolutional layers include zero-padding, so that the output of the network has the same dimensions as the input image and no cropping of the outputs from the layers of the contracting path is needed. The number of convolutional filters applied in the first layer of the contractive path is 32 and the dropout [36] is added in all layers of both the contracting and expansive path, as suggested in [33]. The up-sampling of the outputs in the expansive path is done using transposed convolution.

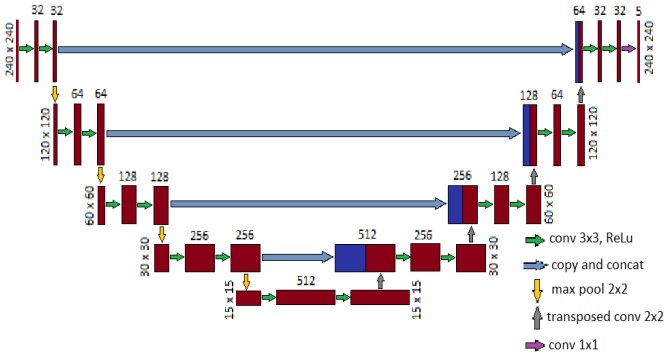

Fig. 1. Implemented U-Net architecture

C. *Implementation details*

The code was written using Python 3.7.4 programing language (Python Software Foundation, SAD). The network model was formed and trained using TensorFlow 1.13.1 with Keras API, with the GPU version installed for the faster and more efficient computing. The program was tested on the PC with Windows 10 Education 64-bit (Microsoft Corporation, Redmond, Washington, USA) operating system, Intel® Core™ i7-5820K (Intel Corporation, Santa Clara, California, USA) processor with 3.30 GHz frequency, 64 GB RAM and NVIDIA GeForce GTX 1060 (NVIDIA Corporation, Santa Clara, California, USA) GPU with 6 GB memory.

As the training dataset of the high-grade glioma scans contains annotations of four tumor structures, while low-grade glioma scans contain annotations of three tumor structures, as they lack enhancing core, it was chosen to train the CNN to segment only high-grade glioma scans, with the aim to segment all four tumor structures. The dataset was divided so that the scans of 170 randomly chosen patients were used for network training and validation, while the scans of the remaining 50 patients were used for testing of the trained network. The network was trained using 140 patients for training and remaining 30 patients for validation. Thus, the training and validation data subset is divided so that 83% of the data are used for training, while 17% are used for the validation of the network parameters. The test set contains 23% of the whole dataset.

As the dataset preprocessing was already done by the BRATS challenge organizers, the only preprocessing step required was the data normalization along each MRI contrast, so that the pixel values belong to the interval [-1, 1], with the zero mean and unit standard deviation, which is a suitable range for the CNN input values. The input of the network is the 4-channel tensor formed of the MRI contrasts. The masks with segmentation labels were transformed into 5-channel matrices, one for each segmentation class, using one-hot encoding principle [37]. The output of the network is the 5-channel map of the same dimensions as the input, containing the probabilities for each pixel in the input to belong to one of the 5 classes: background, necrosis, edema, non-enhancing core or enhancing core. Each pixel is assigned to the class for which the belonging probability is greater than 50%.

The loss function and metrics used for the performance evaluation during the network training are categorical cross-entropy and categorical accuracy [38], which were also chosen for the training of the original U-Net architecture [32]. The activation function after the final convolutional layer in the expansive path of the U-Net is the softmax activation function, which calculates the probability distribution for each pixel in the input image to belong to each of the segmentation classes. The formulas for softmax and categorical cross-entropy loss are given in (1) and (2):

$$softmax(z_i) = \frac{\exp(z_i)}{\sum_j \exp(z_j)} \tag{1}$$

$$J = -\sum_i p_i \log softmax(z)_i \tag{2}$$

where p_i are the weight maps which give more weight to some pixel values during the training process, and z_i represents the unnormalized probability for the pixel x to belong to the segmentation class i [38], as shown in (3):

$$z_i = \log P(y = i \mid x). \tag{3}$$

The segmentation results were evaluated using Dice coefficient, which represents the overlapping proportion of the segmented area and the annotated label:

$$DICE = \frac{2 \cdot |S_g^1 \cap S_t^1|}{|S_g^1| + |S_t^1|}. \tag{4}$$

Here $|S_g^1|$ and $|S_t^1|$ are the areas of pixels belonging to

the considered class in the annotation mask and the segmented result each, while $|S_g^1 \cap S_t^1|$ is the area of pixels belonging to the considered class in both the annotation mask and the segmentation result [5].

The network was trained using Adam optimizer [39] for the maximum of 50 epochs. Regularization techniques used are: validating the network performance on the validation set, learning rate reduction by the coefficient of 0.1 after 3 epochs and early stopping after 10 epochs of non-improving validation loss applied. After the network is trained, the parameters of the saved best model are loaded and the segmentation results are predicted on the training, validation and test sets. Dice coefficient is then calculated for segmentation results for each of the four tumor structures, as well as for the tumor regions consisting of them: tumor core, enhancing tumor and whole tumor.

III. Results and Discussion

The neural network training lasted 70 min. The best evaluation result on the validation dataset occurred in the 4th epoch and the training was stopped 10 epochs later due to early stopping. The best model achieved loss value of approx. 0.03 on the validation set and 0.02 on the training set. The average prediction time per image using the trained model was 8 ms.

TABLE I
NUMBER OF IMAGES CONTAINING TUMOR STRUCTURES

	necrosis	edema	non-enhancing	enhancing
train	4201	10149	7525	6705
valid	1022	2252	1644	1440
test	1379	3666	2634	2284

The number of scans containing each of the tumor structures in the annotation masks for each of the datasets is given in Table 1. Overall, the training set contains 10179 images with at least one tumor structure labeled, the validation set contains 2262 images, while the test set contains 3673 images with at least one tumor structure. Table 1 clearly shows imbalanced data, as the majority of scans in all three sets contain the edema structure, while more than a half of the scans in all sets do not contain a single pixel labeled as necrosis and around a third of the scans do not contain pixels labeled as non-enhancing or enhancing core.

The boxplot diagrams of the Dice coefficient calculated for the tumor structures and tumor regions in all three sets are given in Fig. 2. Median values and mean values are presented as red horizontal lines and green triangles respectively. The boxplot diagrams show better segmentation results for the edema and enhancing core structures than the non-enhancing core and necrosis on all three sets. Dice coefficients achieved for edema and the enhancing core have mean values greater than or equal to 60% and median values greater than or equal to 75% for all three sets, so the segmentation results obtained for these structures can be considered acceptably good. On the other hand, mean values of Dice coefficient obtained for necrotic core are lower than 40% and for the non-enhanced core are around 20% on all three sets, showing poor segmentation results for these structures. The results are expected, as the edema and enhancing core have larger surfaces in the image slices than the necrosis and non-enhancing core, which makes the pixels belonging to the first two structures more common in the image data and makes it more likely for the network to classify them correctly. The mean Dice values for the tumor regions in all the sets are between 0.5 and 0.8, with the highest values achieved for the whole tumor and the lowest values for the tumor core. The mean value achieved on all three datasets for the whole tumor region is greater than 70% and median is greater than 83%. Active tumor region has the mean values greater than or equal to 60% and median greater than or equal to 75%, while the tumor core has the mean value and median each between 50% and 60%, achieved on the test set, and 60% and 80%, achieved on the training set. Achieved mean values greater than 50% and median values greater than or equal to 60% for all tumor regions suggest the successful segmentation of the tumor regions. The achieved segmentation results are comparable to the results of the algorithms available at the BRATS 2015 database website [30]. The greatest limitation of comparing the results of the proposed algorithm with the results in [30] is that in this work two subsets of the high-grade glioma set were used for training and testing of the algorithm, while in the BRATS 2015 challenge the training set consisted of high-grade and low-grade glioma sets, while the separate set without the annotations was used for testing.

An example of the segmentation results for the four tumor structures is given in Fig. 3, while Fig. 4 shows the segmentation results of the tumor regions formed from the structures in Fig. 3. In both figures the segmentation results are overlapping the corresponding annotation masks. Pixels belonging to the annotation masks which were not recognized as the tumor structure by the U-Net are shown in green, pixels predicted as the tumor structure which do not belong to the annotation mask are shown in dark blue, while pixels assigned as tumor structure in both the segmentation result and the annotation mask are presented as bright blue. The achieved values of Dice coefficient are listed under each image in both figures. The best segmentation result was achieved for the edema structure, with the Dice coefficient value of 93%, while the necrotic core was not recognized by the U-Net at all, with the Dice value 0%. It can be noticed that edema has the largest surface of all the structures, while the necrosis has the smallest surface, containing only several pixels in the annotation mask. Furthermore, the incorrectly classified pixels usually belong to the border between the structure area and the background, while pixels inside the area of the annotated structures are usually classified well. Despite the unsuccessful segmentation of the necrotic core and the average segmentation result of the non-enhancing core, with Dice value of 48%, the segmentation of the tumor regions formed from the segmented structures shows good result,

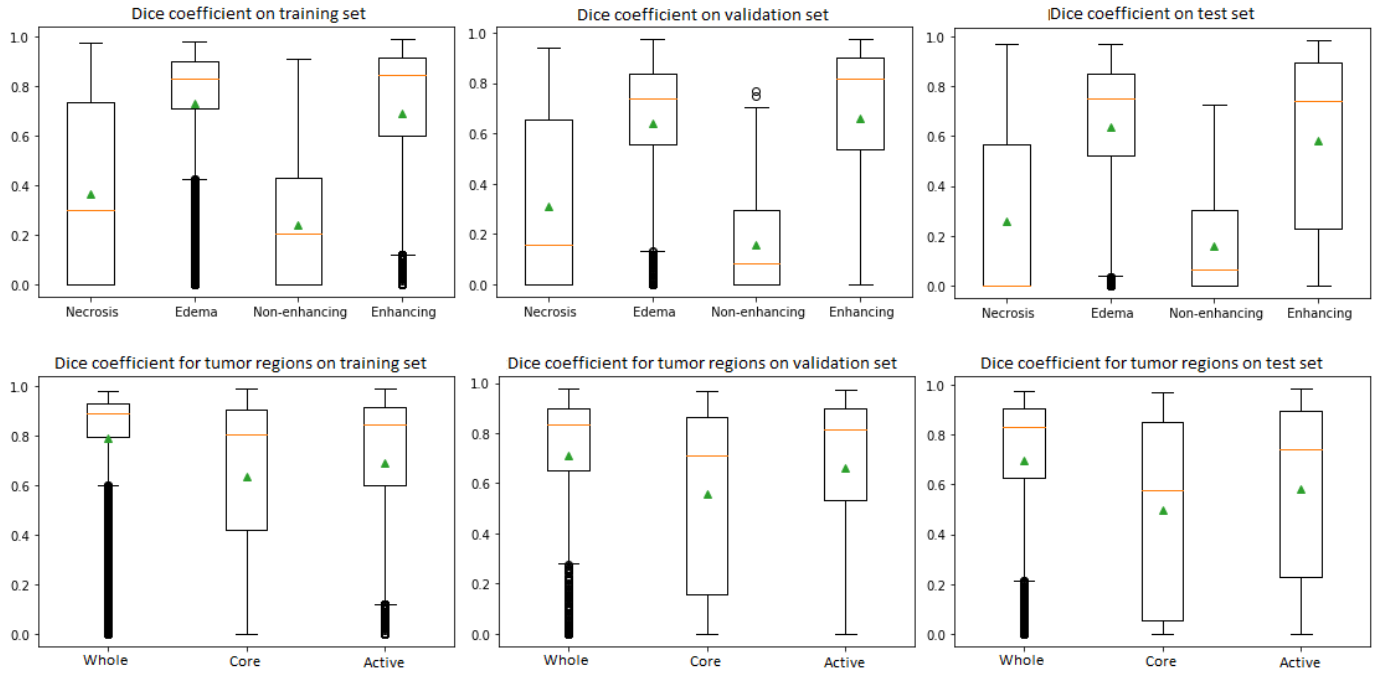

Fig. 2. Boxplot diagram for the Dice coefficient achieved on the tumor structures (1st row) and tumor regions (2nd row).

as shown in Fig. 4, with Dice values of 95% for the whole tumor, 90% for the tumor core and 85% for the active tumor. It is notable that the incorrectly classified pixels usually belong to the borderlines between the different structures.

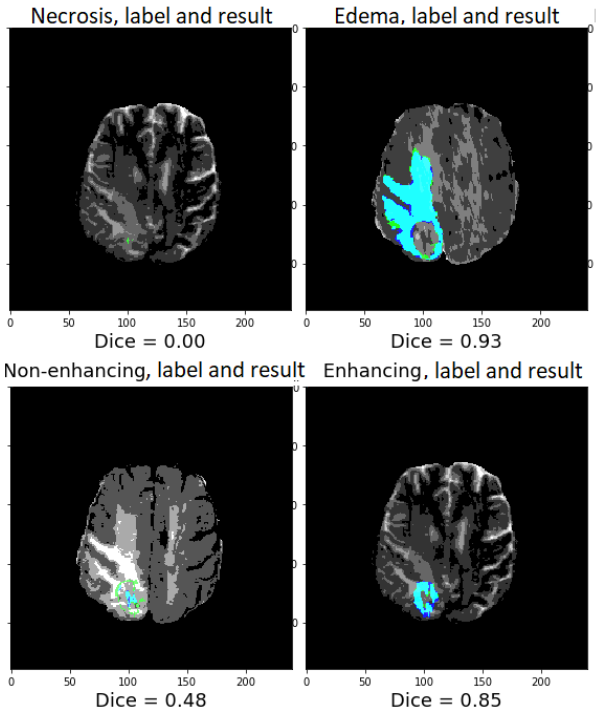

Fig. 3. Example of the segmentation results for tumor structures. Bright blue pixels belong both to the segmented lesion and the annotation mask. Green pixels are ground truth pixels not recognized by the model as tumor structures, while dark blue pixels resemble background pixels incorrectly recognized as tumor structures.

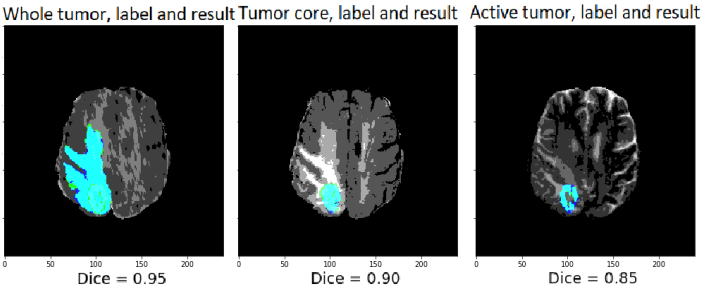

Fig. 4. Example of segmentation results for tumor regions formed from the structures in Fig. 3. The results are presented in the same color order as described in Fig. 3.

IV. Conclusion

In this paper a model of the U-Net CNN architecture was proposed and successfully applied for the segmentation of different tumor structures in the 2D MRI contracts, as well as tumor regions formed from them. The segmentation results are evaluated using Dice coefficient and can be compared to the results proposed at the BRATS 2015 benchmark. It is also shown that the promising segmentation results can be achieved for all tumor regions, with mean Dice values greater than 0.5, despite the poor segmentation results of some of the tumor structures.

Possible improvements could be achieved by modifying the U-Net architecture and tuning some of its parameters as hyper-parameters, such as the number of layers in the contracting and expansive path, number of convolutional layers applied at the input layer of the contractive path, or loss function and metrics used for the evaluation of the network training. Employing data augmentation could create more input images available during the training process and

thus prevent the network from early overfitting. Furthermore, as the consecutive axial slices of the MRI contrasts are mutually dependent, transforming the network architecture so that it extracts information from 3D volumes, instead of 2D images, could also improve results, as proposed in [19, 22].

ACKNOWLEDGMENT

The results presented in this paper were obtained as part of the author's Bachelor's thesis project, defended in September 2019 at School of Electrical Engineering, University of Belgrade. Hereby, the author would like to thank Milica Janković, Assisstant Professor at School of Electrical Engineering, University of Belgrade, the Bachelor's thesis supervisor, for suggestions and comments about this paper.

REFERENCES

[1] PDQ® Adult Treatment Editorial Board. PDQ Adult Central Nervous System Tumors Treatment. Bethesda, MD: National Cancer Institute. Available at: https://www.cancer.gov/types/brain/patient/adult-brain-treatment-pdq. Accessed: Aug, 2020. [PMID: 26389458]

[2] Cancer Research UK, https://www.cancerresearchuk.org/about-cancer/brain-tumours/types, accessed: Aug, 2020.

[3] Cancer Research UK, https://www.cancerresearchuk.org/about-cancer/brain-tumours/types/glioma-adults accessed: Aug, 2020..

[4] D. N. Louis, A. Perry, G. Reifenberger, A. von Deimling, D. Figarella-Branger, W. K. Cavenee, H. Ohgaki, O. D. Wiestler, P. Kleihues, D. W. Ellison, "The 2016 World Health Organization classification of tumors of the central nervous system: a summary," *Acta neuropathol*, vol. *131*, no. *6*, pp. *803-820*, Jun, 2016.

[5] B. H. Menze, A. Jakab, S. Bauer, J. Kalpathy-Cramer, K. Farahani, J. Kirby, Y. Burren, N. Porz, J. Slotboom, R. Wiest, L. Lanczi, E. Gerstner, M. A. Weber, T. Arbel, B. B. Avants, N. Ayache, P. Buendia, D. L. Collins, N. Cordier, J. J. Corso, A. Criminisi, T. Das, H. Delingette, Ç. Demiralp, C. R. Durst, M. Dojat, S. Doyle, J. Festa, F. Forbes, E. Geremia, B. Glocker, P. Golland, X. Guo, A. Hamamci, K. M. Iftekharuddin, R. Jena, N. M. John, E. Konukoglu, D. Lashkari, J. A. Mariz, R. Meier, S. Pereira, D. Precup, S. J. Price, T. R. Raviv, S. M. Reza, M. Ryan, D. Sarikaya, L. Schwartz, H. C. Shin, J. Shotton, C. A. Silva, N. Sousa, N. K. Subbanna, G. Szekely, T. J. Taylor, O. M. Thomas, N. J. Tustison, G. Unal, F. Vasseur, M. Wintermark, D. H. Ye, L. Zhao, B. Zhao, D. Zikic, M. Prastawa, M. Reyes, K. Van Leemput, "The multimodal brain tumor image segmentation benchmark (BRATS)," *IEEE Trans Med Imaging*, vol. *34*, no. *10*, pp. *1993–2024*, Oct, 2015.

[6] https://miccai2020.org/en/, accessed: Aug, 2020.

[7] http://braintumorsegmentation.org/, accessed: Aug, 2020.

[8] A. Davy, M. Havaei, D. Warde-Farley, A. Biard, L. Tran, P. M. Jodoin, A. Courville, H. Larochelle, C. Pal, Y. Bengio, "Brain tumor segmentation with deep neural networks," in Proc. BRATS-MICCAI, pp. *001-004*, Sept, 2014.

[9] G. Urban, M. Bendszus, F. Hamprecht, J. Kleesiek, "Multi-modal brain tumor segmentation using deep convolutional neural networks," in Proc. BRATS-MICCAI, pp. *031-035*, Sept, 2014.

[10] D. Zikic, Y. Ioannou, M. Brown, A. Criminisi, "Segmentation of brain tumor tissues with convolutional neural networks," in Proc. BRATS-MICCAI, pp. *036-039*, Sept, 2014.

[11] B. Pandian, J. Boyle, D. A. Orringer, "Multimodal tumor segmentation with 3D volumetric convolutional neural networks," in Proc. BRATS-MICCAI, pp. *049-052*, Oct, 2016.

[12] S. Chen, C. Ding, C. Zhou, "Brain tumor segmentation with label distribution learning and multi-level feature representation," in Proc. BRATS-MICCAI, pp. *050-053*, Sept, 2017.

[13] M. Havaei, A. Davy, D. Warde-Farley, A. Biard, A. C. Courville, Y. Bengio, C. Pal, P. Jodoin, H. Larochelle, "Brain tumor segmentation with Deep Neural Networks," *Medical Image Analysis*, vol. *35*, pp. *018–031*, Jan, 2017.

[14] K. Kamnitsas, E. Ferrante, S. Parisot, C. Ledig, A. Nori, A. Criminisi, D. Rueckert, B. Glocker, "DeepMedic on brain tumor segmentation," in Proc. BRATS-MICCAI, pp. *018-022*, Oct, 2016.

[15] A. Casamitjana, S. Puch, A. Aduriz, E. Sayrol, V. Vilaplana, "3D convolutional networks for brain tumor segmentation," in Proc. BRATS-MICCAI, pp. *065-068*, Oct, 2016.

[16] A. Karnawat, P. Prasanna, A. Madabushi, P. Tiwari, "Radiomics-based convolutional neural network (RadCNN) for brain tumor segmentation on multi-parametric MRI," in Proc. BRATS-MICCAI, pp. *147-153*, Oct, 2017.

[17] T.K. Lun, W. Hsu, "Brain tumor segmentation using deep convolutional neural network," in Proc. BRATS-MICCAI, pp. *026-029*, Oct, 2016.

[18] S. Dong, "A separate 3D-SegNet architecture for brain tumor segmentation," in Proc. BRATS-MICCAI, pp. *054-060*, Oct, 2017.

[19] X. Feng, C. Meyer, "Patch-based 3D U-Net for brain tumor segmentation," in Proc. BRATS-MICCAI, pp. *067-072*, Oct, 2017.

[20] F. Isensee, P. Kickingereder, W. Wick, M. Bendszus, K. H. Maier-Hein, "Brain tumor segmentation and radiomics survival prediction: contribution to the BRATS 2017 challenge," in Proc. BRATS-MICCAI, pp. *100-107*, Oct, 2017.

[21] G. Kim, "Brain tumor segmentation using deep U-Net," in Proc. BRATS-MICCAI, pp. *154-160*, Oct, 2017.

[22] C. Wang, O. Smedby, "Automatic brain tumor segmentation using 2.5D U-nets," in Proc. BRATS-MICCAI, pp. *292-296*, Oct, 2017.

[23] L. Daia, T. Lib, H. Shuc, L. Zhongd, H. Shena, H Zhub, "Automatic brain tumor segmentation with domain transfer," in Proc. BRATS-MICCAI, pp. *111-118*, Sept, 2018.

[24] M. Cata, A. Casamitjana, I. Sanchez, M. Combalia, V. Vilaplana, "Masked V-Net: an approach to brain tumor segmentation," in Proc. BRATS-MICCAI, pp. *042-049*, Oct, 2017.

[25] R. Hua, Y. Zhang, Q. Huo, Y. Gao, Y. Sun, F. Shi, "Multimodal brain tumor segmentation using cascaded V-Net," in Proc. BRATS-MICCAI, pp. *205-212*, Sept, 2018.

[26] G. Wang, W. Li, S. Ourselin, T. Vercauteren, "Automatic brain tumor segmentation using cascaded anisotropic convolutional neural networks," in Proc. BRATS-MICCAI, pp. *297-303*, Oct, 2017.

[27] D. Lachinov, E. Vasiliev, V. Turlapov, "Glioma segmentation with cascaded Unet: preliminary results," in Proc. BRATS-MICCAI, pp. *272-279*, Sept, 2018.

[28] X. Li, "Fused U-Net for brain tumor segmentation based on multimodal MR images," in Proc. BRATS-MICCAI, pp. *290-297*, Sept, 2018.

[29] K. Kamnitsas, W. Bai, E. Ferrante, S. McDonagh, M. Sinclair, N. Pawlowski, M. Rajchl, M. Lee, B. Kainz, D. Rueckert, B. Glocker, "Ensembles of multiple models and architectures for robust brain tumour segmentation," in Proc. BRATS-MICCAI, pp. *135-146*, Oct, 2017.

[30] https://www.smir.ch/BRATS/Start2015, accessed: Aug, 2020.

[31] M. Kistler, S. Bonaretti, M. Pfahrer, R. Niklaus, P. Buchler, "The Virtual Skeleton Database: An Open Access Repository for Biomedical Research and Collaboration," *J Med Internet Res*, vol. *15*, no. *11*, *e245*, Nov, 2013.

[32] O. Ronneberger, P. Fischer, T. Brox, "U-Net: Convolutional Networks for Biomedical Image Segmentation," in *MICCAI*, *Lecture Notes in Computer Science*, Springer, Cham, vol. *9351*, pp. 234*–241*, Oct, 2015.

[33] A. A. Novikov, D. Lenis, D. Major, J. Hladuvka, M. Wimmer, K. Buhler, "Fully convolutional architectures for multiclass segmentation in chest radiographs," *IEEE Trans on Med Imaging*, vol. *37*, no. *8*, pp. *1865-1876*, Feb, 2018.

[34] B. Kayalibay, G. Jensen, P. van der Smagt, "CNN-based Segmentation of Medical Imaging Data," *ArXiv*, vol. *abs/1701.03056*, n. pag. *24*, Jul, 2017.

[35] H. Dong, G. Yang, F. Liu, Y. Mo, Y. Guo, "Automatic brain tumor detection and segmentation using U-Net based fully convolutional networks", in Proc. Medical Image Understanding and Analysis (MIUA), Edinburgh, UK, Jul,2017.

[36] N. Srivastava, G. Hinton, A. Krizhevsky, I. Sutskever, R. Salakhutdinov, "Dropout: A Simple Way to Prevent Neural Networks from Overfitting", *Journal of Machine Learning Research*, vol. *15*, pp. *1929-1958*, Jun, 2014.

[37] F. Chollet, "Deep Learning for Computer Vision", in *Deep Learning with Python*, New York, USA: Manning Publications Co, 2017, ch. *5*, pp. *119-159*

[38] I. Goodfellow, Y. Bengio A. Courville, "Deep Learning", Cambridge, MA, USA: MIT Press, 2016, URL: http://www.deeplearningbook.org/, accessed: Aug, 2020.

[39] D. Kingma, J. Ba, "Adam: A Method for Stochastic Optimization", in Proc. ICLR, n. pag. *15*, Dec, 2014.